Full Paper

Propellants, Explosives, Pyrotechnics

DOI: 10.1002/prep.201400202

Calcium Sulfate as a Possible Oxidant in "Green" Silicon-based Pyrotechnic Time Delay Compositions

Shepherd M. Tichapondwa,*[a] Walter W. Focke,[a] Olinto Del Fabbro,[a] and Cheryl Kelly[b]

Abstract: Chemical time delay detonators are used to control blasting operations in mines and quarries. Slow burning Si–$BaSO_4$ pyrotechnic delay compositions are employed for long time delays. However, soluble barium compounds may pose environmental and health risks. Hence inexpensive anhydrous calcium sulfate was investigated as an alternative "green" oxidant. EKVI simulations indicated that stoichiometry corresponds to a composition that contains less than 30 wt-% Si. However combustion was only supported in the range of 30–70 wt-% Si. In this range the bomb calorimeter data and burn tests indicate that the reaction rate and energy output decrease with increasing silicon content. The measured burning rates in rigid aluminum elements ranged from 6.9 to 12.5 mm s^{-1}. The reaction product was a complex mixture that contained crystalline phases in addition to an amorphous calcium containing silicate phase. A reaction mechanism consistent with these observations is proposed.

Keywords: Calcium sulfate · Silicon · Time delay · Pyrotechnics

1 Introduction

Delay detonators are extensively employed in mining, quarrying, and other blasting operations. They are used to facilitate sequential initiation of explosive charges in a pattern of boreholes [1]. The timing of the sequential initiation events is carefully chosen in order to control the fragmentation and throw of the rock being blasted. This approach also reduces ground vibration and air blast noise [1]. Both chemical and electronic time delay detonators are used to achieve the required time delays. The simplicity, ruggedness and low cost of pyrotechnic delays make them particularly attractive for high volume mining applications.

Numerous delay compositions, comprising mixtures of fuels and oxidizers, have been developed for different applications [1,2]. Some commercial pyrotechnic compositions contain heavy metal-based oxidizers, e.g. lead, barium, and chromate compounds [3]. Such compounds are deemed environmentally unfriendly and pose a potential health hazard [3b]. This has led to the tightening of health and safety legislation and concerted efforts to find "green" replacements [3a,4]. Silicon is a common fuel used in time delay time detonators [5]. Si–Pb_3O_4 and Si–$BaSO_4$ are currently commercially employed for short-time and long-time delays, respectively. However, both lead and barium based oxidants have been earmarked for replacement, and alternative oxidants for use with silicon are sought. Hence the inexpensive compound anhydrous calcium sulfate was investigated as a potential alternative "green" oxidant.

2 Experimental

2.1 Materials

Ball milled Type 4 silicon was supplied by Millrox. The d_{50} particle size was 2.1 μm (Mastersizer Hydrosizer 2000) and the specific surface area was 11.0 $m^2 g^{-1}$ (Micrometrics Tristar II BET, N_2 at 77 K). Anhydrous calcium sulfate was supplied by Industrial Analytical. It had a d_{50} particle size of 3.8 μm (Mastersizer Hydrosizer 2000) and a specific surface area of 3.5 $m^2 g^{-1}$ (Micrometrics Tristar II BET, N_2 at 77 K). X-ray Diffraction (XRD) analysis of the silicon and calcium sulfate used in the experiments confirmed that both materials were of high purity. Figure 1 shows Scanning Electron Microscopy (SEM) pictures of the calcium sulfate and silicon used in this investigation.

2.2 Preparation Methods

The silicon fuel content in the Si–$CaSO_4$ pyrotechnic composition was varied from 20 to 80 wt-%. The powders were

[a] *S. M. Tichapondwa, W. W. Focke, O. Del Fabbro*
Institute of Applied Materials
Department of Chemical Engineering
University of Pretoria
Lynnwood Road
Pretoria, South Africa
**e-mail: tichapondwa@gmail.com*

[b] *C. Kelly*
Research and Technology
AEL Mining Services
PO Modderfontein, 1645, South Africa

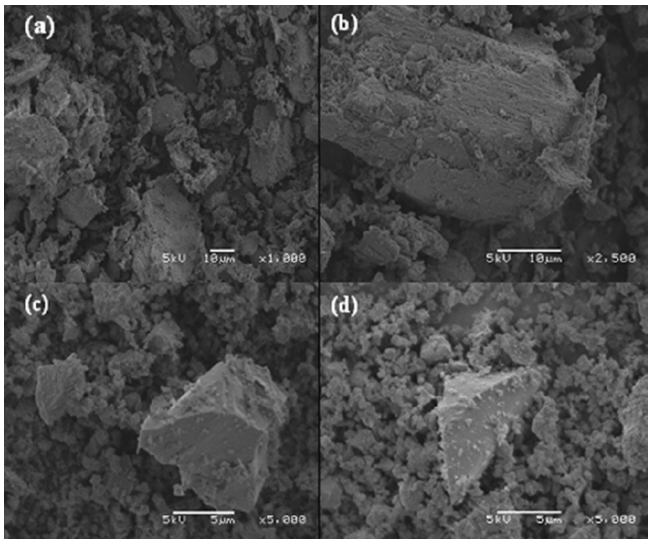

Figure 1. SEM pictures of (a) and (b) calcium sulfate; (c) and (d) silicon.

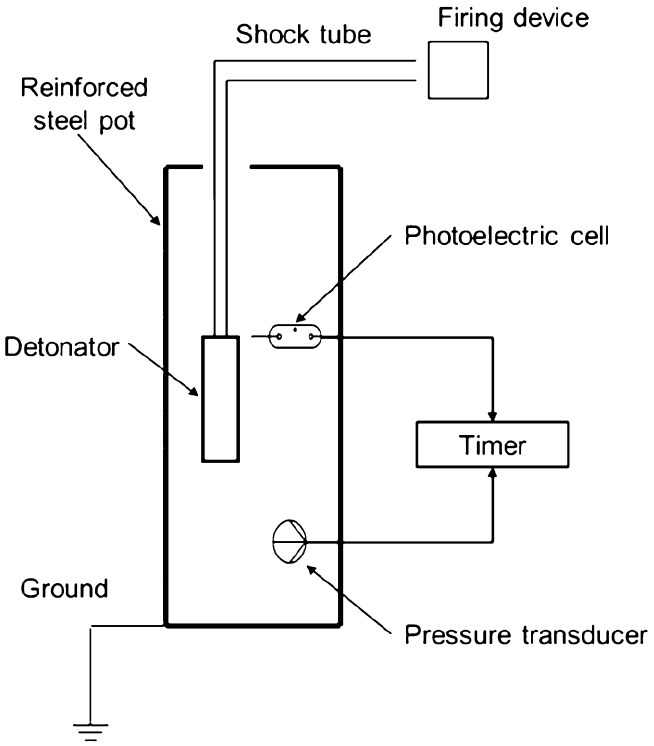

Figure 2. Firing and timing schematic used for burning rate measurements.

mixed by brushing them several times through a 75 μm sieve. The compositions were pressed into 25 mm long aluminum tubes with an internal diameter of 3.6 mm and a wall thickness of 1.45 mm. The filling process started with two increments of a proprietary starter composition pressed with a 100 kg load. This was followed by repeated steps of adding two increments of the delay composition and pressing it with the same load until the tube was filled.

2.3 Burning Rate Measurements

The burning rates were determined using commercial detonator assemblies. The detonators comprised an initiating shock tube coupled to a rigid aluminum time delay element contained in an aluminum shell. This outer shell contained increments of lead azide primary explosive and pentaerythritol tetranitrate (PETN) as the secondary explosive. The way the actual delay time was determined is illustrated in Figure 2. The shock tube was ignited by the firing device and the resultant flash was recorded by the photoelectric cell. This signal was sent to the timer as the initiating signal. After detonation, the pressure transducer sent another signal to the timer, which marked the end point of the timing sequence [6].

2.4 Characterization

Thermogravimetric analysis (TGA) was performed with a Mettler Toledo A851 TGA/SDTA using the dynamic method. About 15 mg of powder sample was placed in an open 70 μL alumina pan. Temperature was scanned from 25 to 1300 °C at a rate of 10 °C min^{-1} with nitrogen flowing at a rate of 50 mL min^{-1}. Three runs were carried out for each sample.

Enthalpy measurements were carried out with a Parr 6200 calorimeter utilizing a 1104B 240 mL high strength bomb. Tap compacted test compositions (2 g) were initiated using 0.2 g of a proprietary starter. It was ignited with an electrically heated 30 gauge nichrome wire. The tests were carried out in a 3.0 MPa helium atmosphere. The variation of pressure with time was followed using a National Instruments piezoelectric transducer. A Parr Dynamic Pressure Recording System was used for data collection. The recording frequency was 5 kHz and 30000 data points were captured per test. Each composition was tested at least three times.

X-ray Diffraction (XRD) measurements were performed with a BRUKER D8 ADVANCE diffractometer with 2.2 kW Cu-K_α radiation ($\lambda = 0.154060$ nm) fitted with a LynxEye detector with a 3.7° active area. Samples were scanned in reflection mode in the angular range of 2° to 70° 2θ at a rate of 0.01° s^{-1}. The generator settings were 40 kV and 40 mA. Data processing and analysis were carried out using the BRUKER DIFFRAC^{Plus}–EVA evaluation program. Quantitative XRD analyses were performed according to the Rietveld method using DIFFRAC^{Plus} TOPAS software. The powdered residues were spiked with known proportions of corundum, a highly crystalline material. This made it possible to determine the amorphous content from the recorded diffractograms using the Rietveld method as discussed by Ward and French [7].

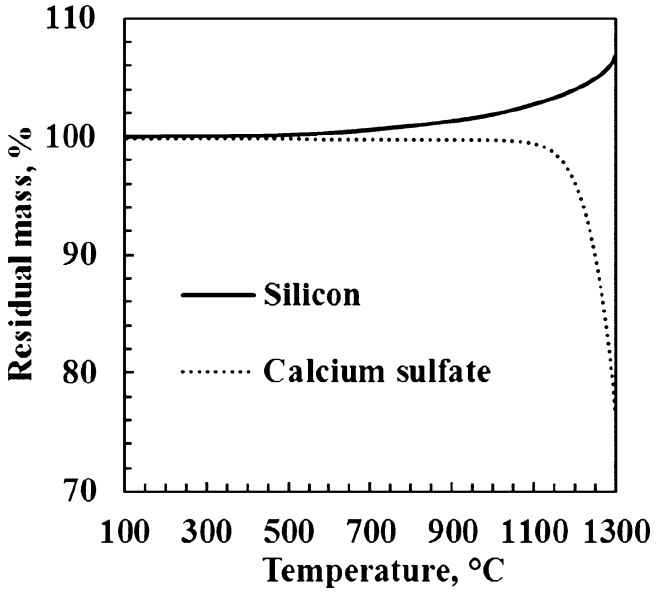

Figure 3. TGA results for silicon and calcium sulfate recorded in a nitrogen atmosphere.

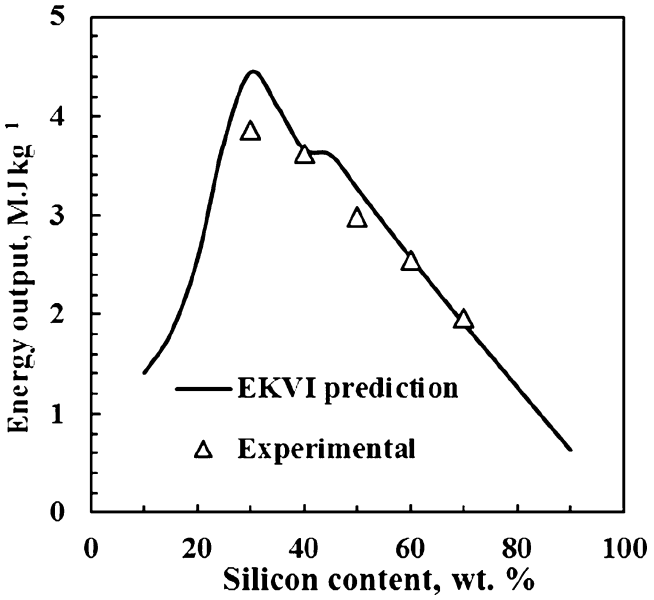

Figure 4. Comparison of experimental energy outputs obtained with the bomb calorimeter in a helium atmosphere with EKVI simulations for Si–$CaSO_4$.

Single point sulfur analyses were performed with an Eltra CS 800 double dual range carbon-sulfur analyzer. Samples of the reaction products weighing ca. 0.2 g were milled and sieved to < 75 μm. The samples were homogenized by slow rotation in a ceramic crucible with iron and tungsten chips. The instrument was calibrated using the Euronorm-CRM 484-1 Whiteheart malleable iron, Euronorm-CRM 058-2 sulfur steel and Euronorm-CRM 086-1 carbon steel standards. The instrument stability was monitored using the Council for Geoscience laboratory in-house soil reference standards. The sulfur detection limit was 0.009 wt-%.

3 Results

3.1 Thermal Stability of Reactants

Figure 3 shows the thermal stability of the silicon and calcium sulfate in a nitrogen atmosphere. The silicon showed no significant change in mass between 25 °C and 600 °C. However, a mass increase associated with the formation of silicon nitride was noted above 600 °C. The anhydrous $CaSO_4$ was stable beyond 1000 °C with the onset of decomposition above 1100 °C. Previous TGA results indicate that the onset temperature for the decomposition falls in the range of 1080 °C to 1300 °C [8]. Depending on the partial pressures of SO_3, SO_2, and O_2, the thermal decomposition of anhydrous calcium sulfate takes place according to either Equation (1) or Equation (2) [9]. Complete decomposition to CaO results in a theoretical mass loss of 59 %.

$$CaSO_4(s) \rightarrow CaO(s) + SO_2(g) + {}^1/_2O_2(g) \quad (1)$$

$$CaSO_4(s) \rightarrow CaO(s) + SO_3(g) \quad (2)$$

3.2 Experimental and Theoretical Energy Output Measurements

The effect of the fuel content on the energy output of the Si–$CaSO_4$ formulations is shown in Figure 4 and Table 1. Ignition and propagation was only sustained in the range of 30 to 70 wt-% silicon. Compositions containing 20 or 80 wt-% silicon failed to propagate. The energy output decreases approximately linearly with increasing silicon content. The outputs ranged from 3.87 to 1.97 MJ kg^{-1}. The 30 wt-% silicon composition, which is the closest to stoichiometry, had the highest energy output [10]. Thermochemical predictions made using the EKVI thermodynamic software package over the range of 10 to 90 wt-% silicon are also shown in Figure 4. The calculated exothermicity values from the EKVI program agreed reasonably well with the measured values. This suggests that the metal-oxidant reaction proceeded via the thermodynamically favored pathway. Table 2 shows the constant-volume adiabatic reaction tem-

Table 1. Energy output and peak pressures, times to reach the peak pressure, and the maximum pressurization rates extracted from the relative pressure-time profiles measured in the bomb calorimeter.

	Si content [wt-%]				
	30	40	50	60	70
Energy output [MJ kg^{-1}]	3.87	3.62	2.98	2.55	1.97
P_{max} [MPa]	2.06	1.76	1.41	0.65	0.49
t_{max} [s]	1.20	1.28	1.28	1.84	2.08
dP/dt_{max} [MPa s^{-1}]	4.45	3.08	1.82	0.60	0.40

Table 2. Calculated maximum pressure differences assuming that all the $CaSO_4$ in the samples placed in the bomb calorimeter decomposed according to either Equation (1) or (2), and adiabatic reaction temperatures predicted with the EKVI thermochemistry simulations.

	Si content [wt-%]				
	30	40	50	60	70
Equation (1) [MPa]	0.16	0.14	0.11	0.09	0.07
Equation (2) [MPa]	0.11	0.09	0.08	0.06	0.05
Adiabatic reaction temperature [°C]	1684	1429	1300	1058	810

peratures calculated with the EKVI code. There is a clear dependency of the adiabatic temperature on stoichiometry with the 30 wt-% silicon composition predicted to have the highest reaction temperature of 1684 °C.

3.3 Pressure – Time Analysis

Time-dependent changes in pressure, relative to the initially applied helium pressure of 3.0 MPa, are shown in Figure 5. A summary of the information extracted from the pressure-time relationships is presented in Table 1. There are clear trends with the rate of pressure rise as well as the maximum peak pressure decreasing with increasing silicon content. This correlates with the observation of decreasing energy with increasing silicon content in this composition range. There was a noticeable time delay before the pressure rose. This time lag was almost independent of the fuel content of the composition. Figure 5 reveals higher residual pressure differences at the end of the six second pressure test for the 30 and 40 wt-% silicon formulations compared to the other three compositions. This could either be due to a higher residual temperature caused by the higher energy outputs or to the generation of more gas. The residual pressure differences, after cooling to room temperature, were calculated assuming that the entire calcium sulfate present in the test sample decomposed completely according to either Equation (1) or (2) (Table 2). Maximum pressure differences of 0.16 and 0.11 MPa, respectively, were found for the 30 wt-% composition. The theoretical results are considerably lower than all the experimentally measured residual pressures after six seconds. This suggests that the higher differential pressures were caused by residual heating effects.

3.4 Burning Rates

Figure 6 shows the effect of stoichiometry on the burning rate of the Si–$CaSO_4$ system. The burning rate decreased with increasing silicon content. The composition containing 30 wt-% silicon burned fastest (12.5 mm s^{-1}), whilst the 70 wt-% silicon composition was the slowest (6.9 mm s^{-1}). This burning rate is similar to the burning rate of Si–$BaSO_4$ compositions (4–9 mm s^{-1}) [11] but is much slower than the range reported for Si–Pb_3O_4 compositions (40–257 mm s^{-1}) [12].

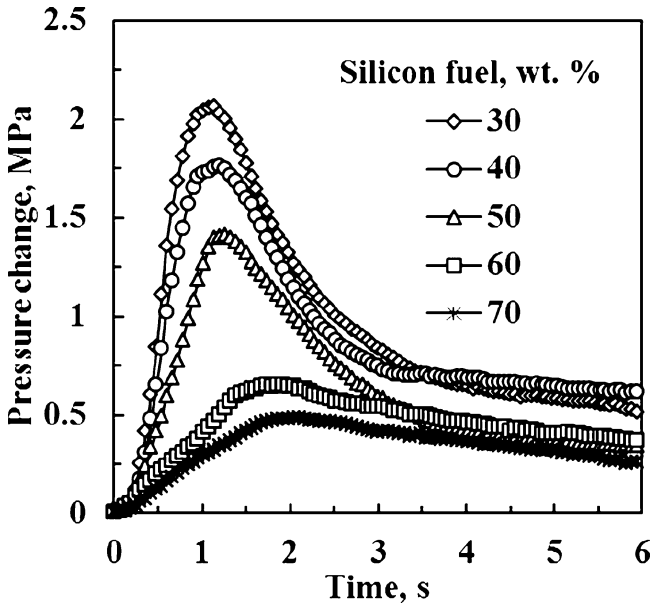

Figure 5. Pressure increase with time for different Si–$CaSO_4$ compositions during the bomb calorimetry experiments in a helium atmosphere.

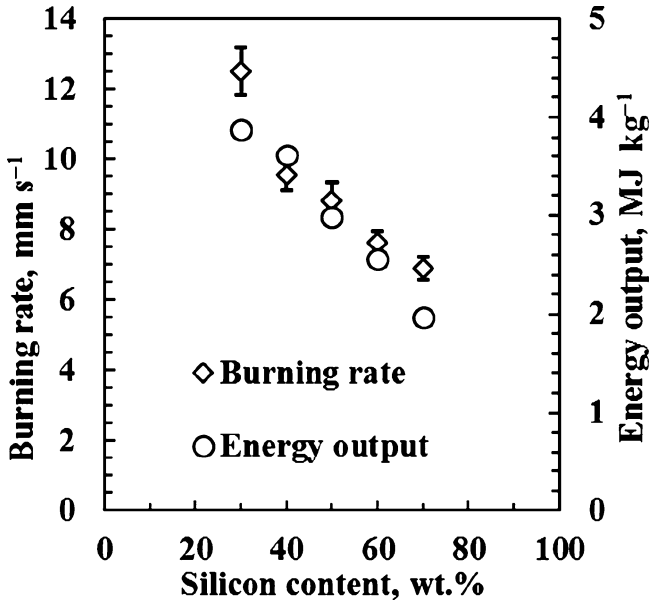

Figure 6. The effect of fuel content on the burning rate and energy output of Si–$CaSO_4$ compositions.

Table 3. Quantitative analysis of the reaction products identified from the Si–$CaSO_4$ pyrotechnic composition using XRD as well as an analysis of the total sulfur content in the solid products.

		Si content [wt-%]				
		30	40	50	60	70
Phase						
Silicon	Si	2.7	17.7	26.8	36.3	41.1
Quartz	SiO_2	2.6	4.0	4.9	1.1	1.2
Pseudowollastonite	$Ca_3(SiO_3)_3$	19.2	25.5	13.6	9.8	10.4
Calcium sulfide	CaS	9.2	14.4	13.6	10.7	1.9
Bismuth	Bi	0.6	2.4	1.3	1.5	1.7
Bismuthinite	Bi_2S_3	1.2	1.9	1.3	1.1	0.7
Amorphous[a)]		64.5	34.1	38.5	39.5	43.1
Si/Ca ratio						
Reagents		2.08	3.23	4.84	7.27	11.3
Crystalline phase		1.04	2.19	3.77	5.99	13.6
Amorphous phase		3.02	6.64	7.47	10.2	9.15
Sulfur analysis [wt-%]		9.9	5.5	5.3	4.0	3.1
Gas evolved [$cm^3 g^{-1}$]		51.2	63.5	48.0	39.8	28.8

a) Mainly silica.

Figure 6 also shows that the burning rate and the energy output decrease in tandem as the fuel content increases. According to Khaikin and Merzhanov [13] the burning rate varies inversely with the square root of the energy output. However, according to Hill et al. [14], the burning rate should be directly proportional to the energy output and this is roughly the case for the presented data.

3.5 XRD Analysis of Reaction Products

Quantitative X-ray diffraction (XRD) analysis was performed on the reaction products (see Table 3). This information was used to deduce a reaction mechanism and to establish whether the combustion products were environmentally benign. The major crystalline products detected were calcium sulfide (CaS), pseudowollastonite [$Ca_3(SiO_3)_3$], quartz (SiO_2), and unreacted silicon. Trace amounts of bismuth metal and bismuthinite (Bi_2S_3) were also detected. These impurities derived from the proprietary bismuth oxide based starter that was used to ignite the various formulations. These results also revealed the presence of a significant amount of an amorphous phase in the reaction products. No unreacted calcium sulfate was detected. This was expected since gypsum thermally degrades below the high pyrotechnic reaction temperatures.

Table 3 also reports the sulfur analysis of the solid reaction residues. Sulfur was essentially retained the form of calcium sulfide with minute amounts present in the amorphous phase. A sulfur mass balance enabled the determination of the amount of gas produced during the reaction assuming no impurities in the reactants and that SO_2 is the only gas evolved. Depending on the stoichiometry, the gas evolved at standard temperature and pressure conditions ranged from 29.2 to 57.5 $cm^3 g^{-1}$. This is considerably higher than the 10 $cm^3 g^{-1}$ generally taken as the upper limit for classification as a gasless composition [15].

Mass balances on the other elements were also carried out. In particular, the Si:Ca ratio in the amorphous phase exceeded three for all the compositions. This indicates that the amorphous phase was predominantly composed of silica (SiO_2).

Table 4, Figure 7, and Figure 8 provide details of the EKVI simulation results for the Si–$CaSO_4$ formulation. A comparison of the data reveals that the experimental silicon conversions were similar for the 30–50 wt-% silicon compositions. However, the remaining compositions showed higher

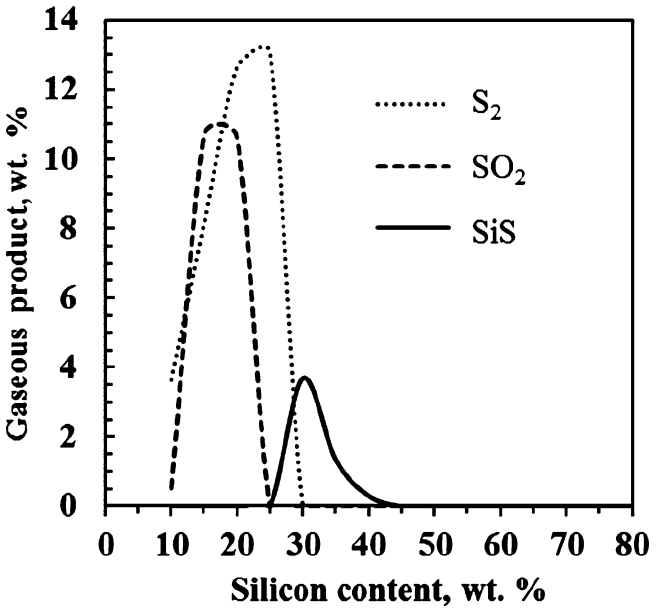

Figure 7. Gaseous products released during the combustion of the Si–$CaSO_4$ pyrotechnic composition predicted with the EKVI thermodynamics software.

Table 4. Major reaction products of the Si–$CaSO_4$ composition predicted using EKVI thermodynamics code under adiabatic conditions.

Formula	10	20	30	40	50	60	70	80	90
SO_2(g)	0.5	10.6	–	–	–	–	–	–	–
S_2(g)	3.7	12.7	–	–	–	–	–	–	–
SiS(g)	–	–	3.7	0.3	–	–	–	–	–
Si(s)	–	–	0.1	15.2	29.4	43.5	57.6	71.8	85.9
SiO_2(s)	12.2	19.5	57.5	52.6	44.1	35.3	26.5	17.7	8.8
CaS(s)	–	–	32.9	31.5	26.5	21.2	15.9	10.6	5.3
$Ca_3Si_2O_7$(s)	24.3	57.2	5.9	0.5	0.1	–	–	–	–
$CaSO_4$(s)	59.4	–	–	–	–	–	–	–	–
Total	100	100	100	100	100	100	100	100	100

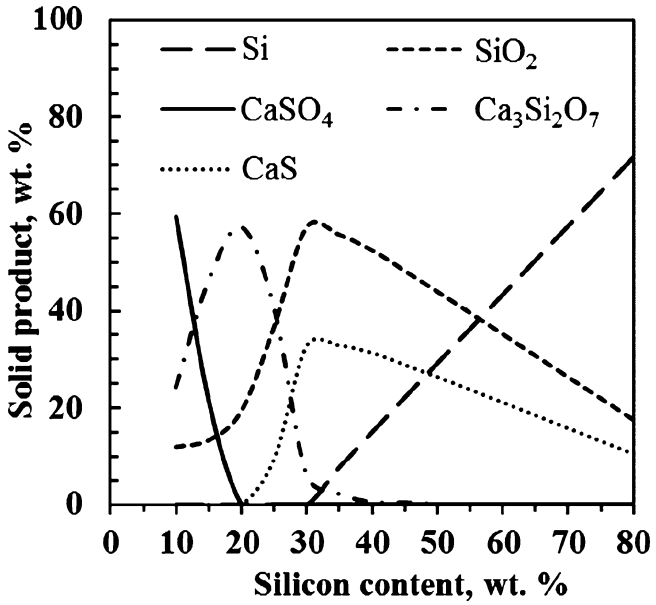

Figure 8. Solid products obtained during the combustion of the Si–$CaSO_4$ pyrotechnic composition predicted with the EKVI thermodynamics software.

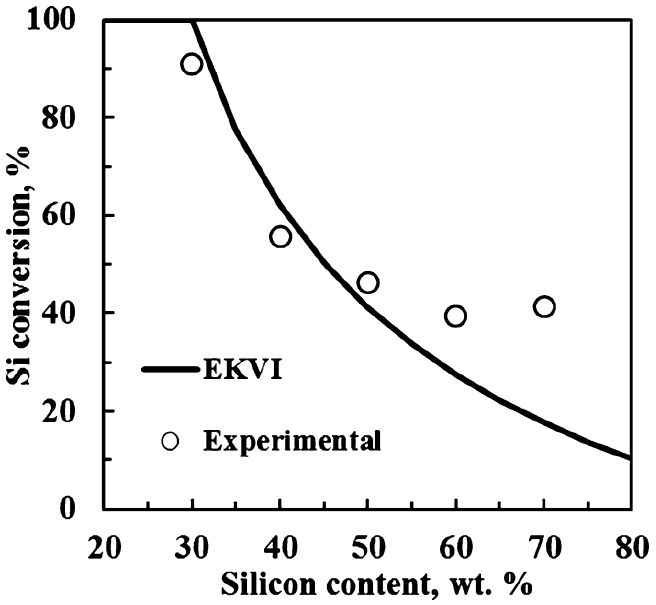

Figure 9. Comparison of the conversion of silicon based on XRD reaction products and the reaction products predicted using the EKVI thermodynamics software.

conversions than the predictions of the EKVI thermochemistry simulations (Figure 9).

The reaction product spectra predicted with the EKVI were similar to those found experimentally. However, according to the EKVI simulation, all the test compositions essentially qualify as "gasless" since the predicted amount of gas produced was minimal. Exceptions were seen in the case of the low silicon content formulations i.e. 10 and 20 wt-% Si, where quantifiable amounts of SO_2(g) and elemental S_2(g) were predicted. In the case of 30 wt-% silicon composition SiS gas formation was predicted. The major solid phases predicted were SiO_2, CaS, $Ca_3Si_2O_7$, and unreacted silicon. The program predicted complete conversion of the $CaSO_4$ to CaS. However, $Ca_3Si_2O_7$ was only prominent in the 10 and 20 wt-% Si compositions. It should be noted that the EKVI database includes wollastonite $CaSiO_3$ but does not contain pseudowollastonite; this will influence the predictions made with the software.

4 Discussion

Pseudowollastonite and calcium sulfide were the dominant crystalline phases in the residue left by the Si–$CaSO_4$ reaction. The former is a high temperature polymorph of wollastonite ($CaSiO_3$). Gladun and Bashaeva [16] performed a thermodynamic analysis of possible reactions for high temperature synthesis of wollastonite. They found that it can be obtained in the temperature range 1000 to 1400 °C. Their results, the presented XRD and TGA data as well as the findings of Mu and Zaremba [17] can be explained by the set of reactions of the Si–$CaSO_4$ pyrotechnic composition proposed in Equation (3), Equation (4), Equation (5), and Equation (6):

$$CaSO_4 + 2Si \rightarrow CaS + 2SiO_2 \quad (3)$$

$$CaSO_4 \rightarrow CaO + SO_2 + {}^1/_2O_2 \quad (4)$$

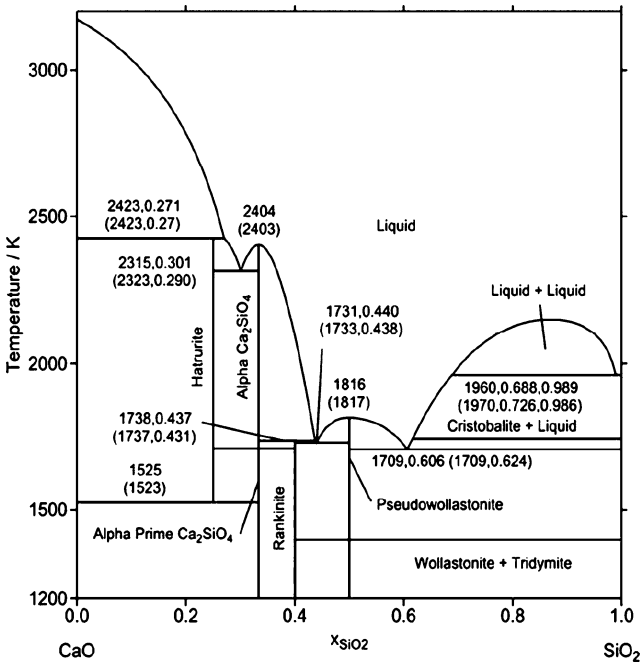

Figure 10. Phase diagram for the system CaO-SiO_2 reproduced with permission from the authors of reference [18].

$$Si + O_2 \rightarrow SiO_2 \quad (5)$$

$$SiO_2 + CaO \rightarrow CaSiO_3 \quad (6)$$

Figure 10 shows a CaO–SiO_2 phase diagram calculated using the MTDATA software developed by Davies et al. [18]. The phase diagram shows that several compounds or compound combinations are formed at different temperatures and CaO–SiO_2 ratios. A mass balance, which was carried out to establish the Si : Ca ratio, revealed that the amorphous phase is predominantly made up of SiO_2. Table 3 shows that the silicon to calcium ratio in the amorphous phase of all the residues was much higher than the 1 : 1 ratio expected for wollastonite, varying from 3.02 to 10.2. These correspond to SiO_2 mol fractions of 0.75 to 0.91 in Figure 10. This means that the formation of the pseodowollastonite and the amorphous phase identified and quantified by XRD analysis can be attributed to a combination of Equation (5) and Equation (6). It also implies that these phases were most likely fixed in the square temperature-composition region second from below and on the far right hand side of the phase diagram in Figure 10. It is worth noting that the reported solid product analysis only provides an idea of the actual reaction products since the analysis was performed at room temperature while the theoretical adiabatic temperature can reach 1684 °C. Furthermore, the cooling rate experienced by the residue may have influenced the distribution between crystalline and the amorphous phases.

5 Conclusions

Calcium sulfate was shown to be a viable oxidant for silicon in slow-burning time delay compositions. The energy outputs, pressure-time profiles, and burning rate measurements all showed a general trend of decreasing with increasing silicon content. XRD analysis of the reaction products revealed that the products were a composite mixture of crystalline and amorphous phases. The fair agreement between the EKVI simulation results and the present experimental data suggests that the reaction proceeds by the thermodynamically favored pathway. Both the reactants and the products of the composition tested are environmentally benign.

Acknowledgments

This work is based on the research supported in part by AEL Mining Service and by the National Research Foundation of South Africa (Grant 83874). The opinions, findings and conclusions or recommendations expressed in this publication are those of the authors, and neither AEL Mining Services nor the NRF accept any liability whatsoever in this regard.

References

[1] M. W. Beck, J. Flanagan, *Delay Composition and Device*, US Patent 5, 147, 476, Imperial Chemical Industries PLC, London, UK, **1992**.

[2] A. L. Davitt, K. A. Yuill, *Delay Composition for Detonators*, US Patent, 4, 374, 686, CXA Ltd/CXA Ltd., North York, Canada, **1983**.

[3] a) C. K. Wilharm, A. Chin, S. K. Pliskin,Thermochemical Calculations for Potassium Ferrate (VI), K_2FeO_4, as a Green Oxidizer in Pyrotechnic Formulations, *Propellants Explos. Pyrotech.* **2013**, 35, 1; b) J. C. Poret, A. P. Shaw, C. M. Csernica, K. D. Oyler, J. A. Vanatta, G. Chen, Versatile Boron Carbide-Based Energetic Time Delay Compositions, *ACS Sustainable Chem. Eng.* **2013**, *1*, 1333.

[4] a) G. Steinhauser, T. M. Klapötke, "Green" Pyrotechnics: A Chemists' Challenge, *Angew. Chem. Int. Ed.* **2008**, *47*, 3330; b) R. Cramer, Green Energetic Materials: An Overview, *38th International Pyrotechnics Seminar*, Denver, CO, USA, 10–15 June, **2012**.

[5] a) R. A. Rugunanan, *Intersolid Pyrotechnic Reactions of Silicon*, PhD Thesis, Rhodes University, Grahamstown, South Africa, **1991**; b) I. Ricco, W. Focke, C. Conradie, Alternative Oxidants for Silicon Fuel in Time-Delay Compositions, *Combust. Sci. Technol.* **2004**, *176*, 1565; c) L. Kalombo, O. Del Fabbro, C. Conradie, W. W. Focke, Sb_6O_{13} and Bi_2O_3 as Oxidants for Si in Pyrotechnic Time-Delay Compositions, *Propellants Explos. Pyrotech.* **2007**, *32*, 454.

[6] K. Ilunga, O. Del Fabbro, L. Yapi, W. W. Focke, The Effect of Si–Bi_2O_3 on the Ingnition of the Al–CuO Thermite, *Powder Technol.* **2011**, *205*, 97.

[7] C. R. Ward, D. French, Determination of Glass Content and Estimation of Glass Composition in Fly Ash using Quantitative X-ray Diffractometry, *Fuel* **2006**, *85*, 2268.

[8] a) E. Newman, Behavior of Calcium Sulfate at High Temperatures, *J. Res. Nat. Bur. Stand.* **1941**, *27*, 191; b) E. Van der

Merwe, C. Strydom, J. Potgieter, Thermogravimetric Analysis of the Reaction Between Carbon and $CaSO_4 \cdot 2H_2O$, Gypsum and Phosphogypsum in an Inert Atmosphere, *Thermochim. Acta* **1999**, *340*, 431.

[9] K. H. Stern, E. L. Weise, *High Temperature Properties and Decomposition of Inorganic Salts. Part 1. Sulfates*. No. NSRDS-NBS-7, National Standard Data System, **1996**.

[10] B. Berger, Parameters Influencing the Pyrotechnic Reaction, *Propellants Explos. Pyrotech.* **2005**, *30*, 27.

[11] M. Beck, *A Preliminary Investigation into the Si–$BaSO_4$ Combustion Mechanism*, Report No. 684, ICI Explosives Group, Ardeer Site, UK, **1989**.

[12] J. A. Goodfield, G. J. Rees, Pyrotechnic Reaction of Lead Monoxide and Silicon: Measurement of Reaction Temperature, *Fuel* **1981**, *60*, 151.

[13] B. Khaikin, A. Merzhanov, Theory of Thermal Propagation of a Chemical Reaction Front, *Combust. Explos. Shock Waves (Eng. Transl.)* **1966**, *2*, 22.

[14] R. A. W. Hill, L. E. Sutton, R. B. Temple, A. White, Slow Self-Propagating Reaction in Solids, *Research* **1950**, *5*, 569.

[15] E. Charsley, C.-H. Chen, T. Boddington, P. Laye, J. Pude, Differential Thermal Analysis and Temperature Profile Analysis of Pyrotechnic Delay Systems: Ternary Mixtures of Silicon, Boron and Potassium Dichromate, *Thermochim. Acta* **1980**, *35*, 141.

[16] V. Gladun, L. Bashaeva, High Temperature Synthesis of Wollastonite and Possibilities of its Use in Pyrotechnics, *21st International Pyrotechnics Seminar*, Moscow, Russia, 11–15 September, **1995**.

[17] J. Mu, G. Zaremba, Effect of Carbon and Silica on the Reduction of Calcium Sulfate, *Thermochim. Acta* **1987**, *114*, 389.

[18] R. Davies, A. Dinsdale, J. Gisby, J. Robinson, S. Martin, MTDATA-Thermodynamic and Phase Equilibrium Software from the National Physical Laboratory, *CALPHAD Comput. Coupling Phase Diagrams Thermochem.* **2002**, *26*, 229.

Received: August 25, 2014
Revised: October 14, 2014
Published online: November 24, 2014

